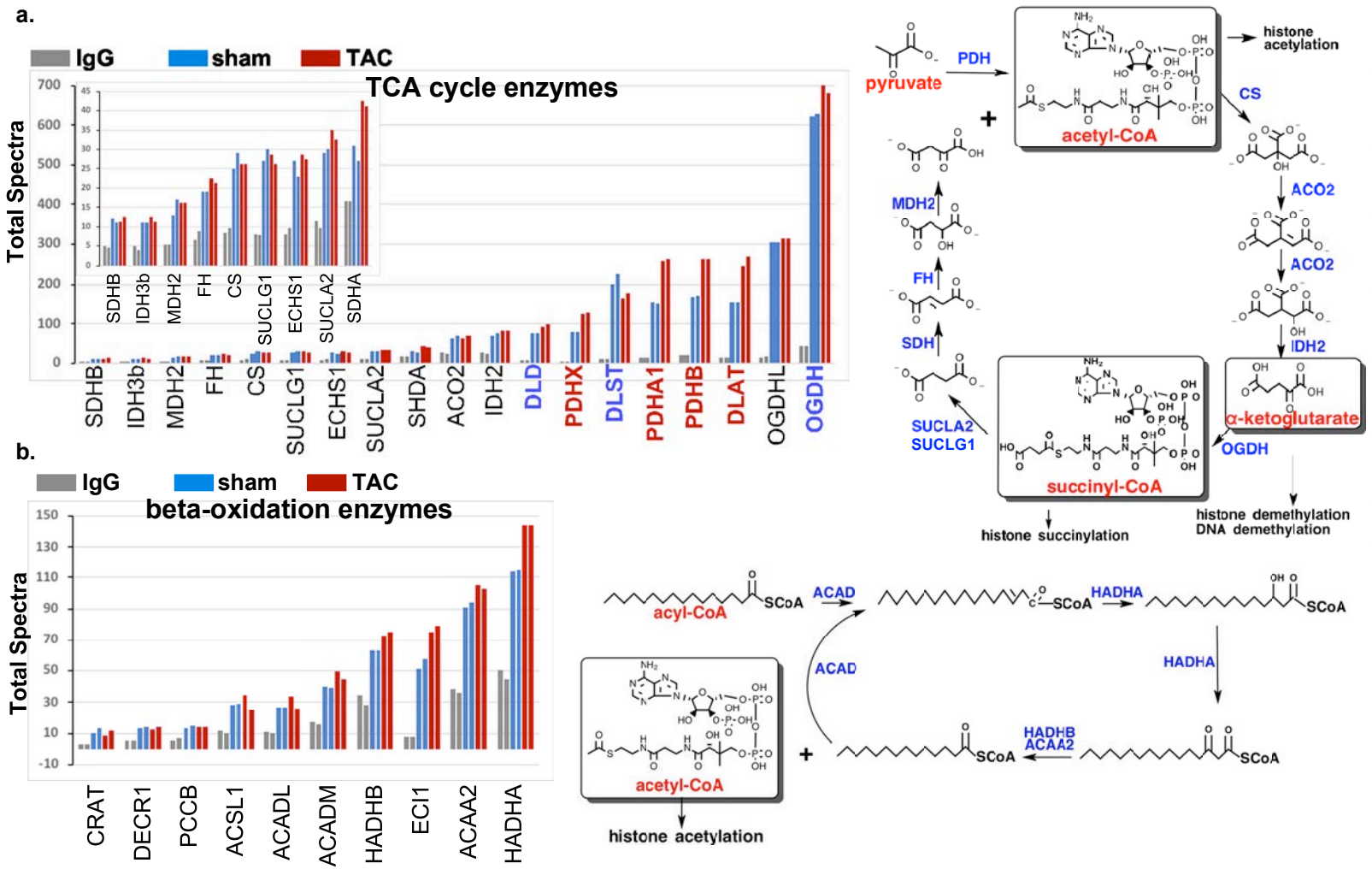

Figure 1S (a-b). Proteins that co-precipitated with H2A.Z-bound chromatin in the RIME assay. RIME with anti-H2A.Z or a control IgG was performed on nuclei from a pool of 10 hearts each, from mice subjected to a sham or a transverse aortic constriction operation. **a-b.** Total spectra identified in the IgG, sham, and TAC samples were plotted. These include those with a cutoff of equal or greater than 2-fold enrichment v. control IgG, after normalization to the IgG C chain region spectra that were detected in each sample. Data were grouped as **a**. TCA cycle enzymes, also represented in blue in the diagram on the right. Note, all the subunits for the PDH (red labels) and OGDH (blue labels) complexes were detected in the RIME assay. **b.** beta-oxidation spiral enzymes, also represented in blue in the diagram on the right.

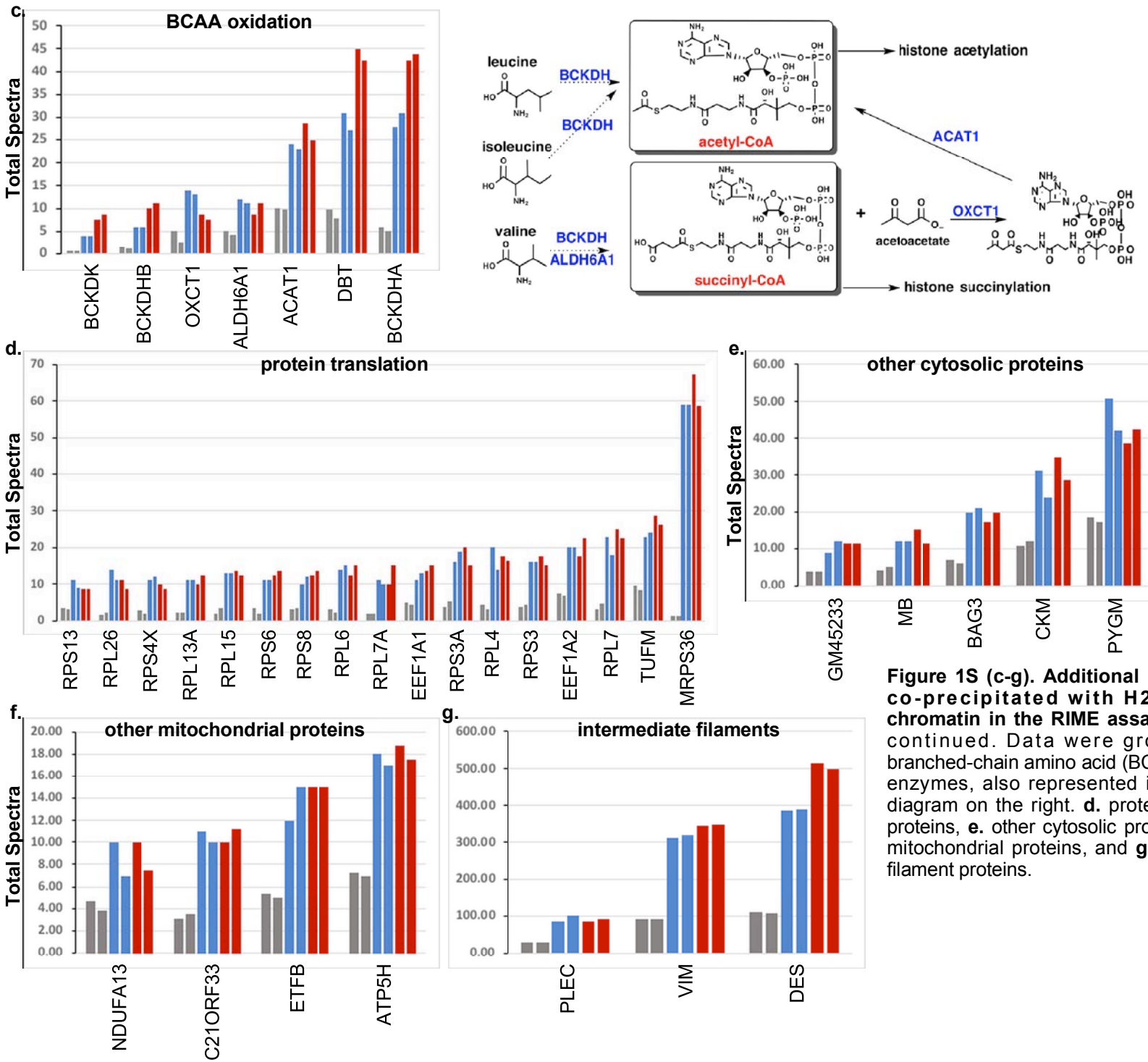

Figure 1S (c-g). Additional proteins that co-precipitated with H2A.Z-bound chromatin in the RIME assay. RIME data continued. Data were grouped as **c**. branched-chain amino acid (BCAA) oxidation enzymes, also represented in blue in the diagram on the right. **d.** protein translation proteins, **e.** other cytosolic proteins, **f.** other mitochondrial proteins, and **g.** intermediate filament proteins.

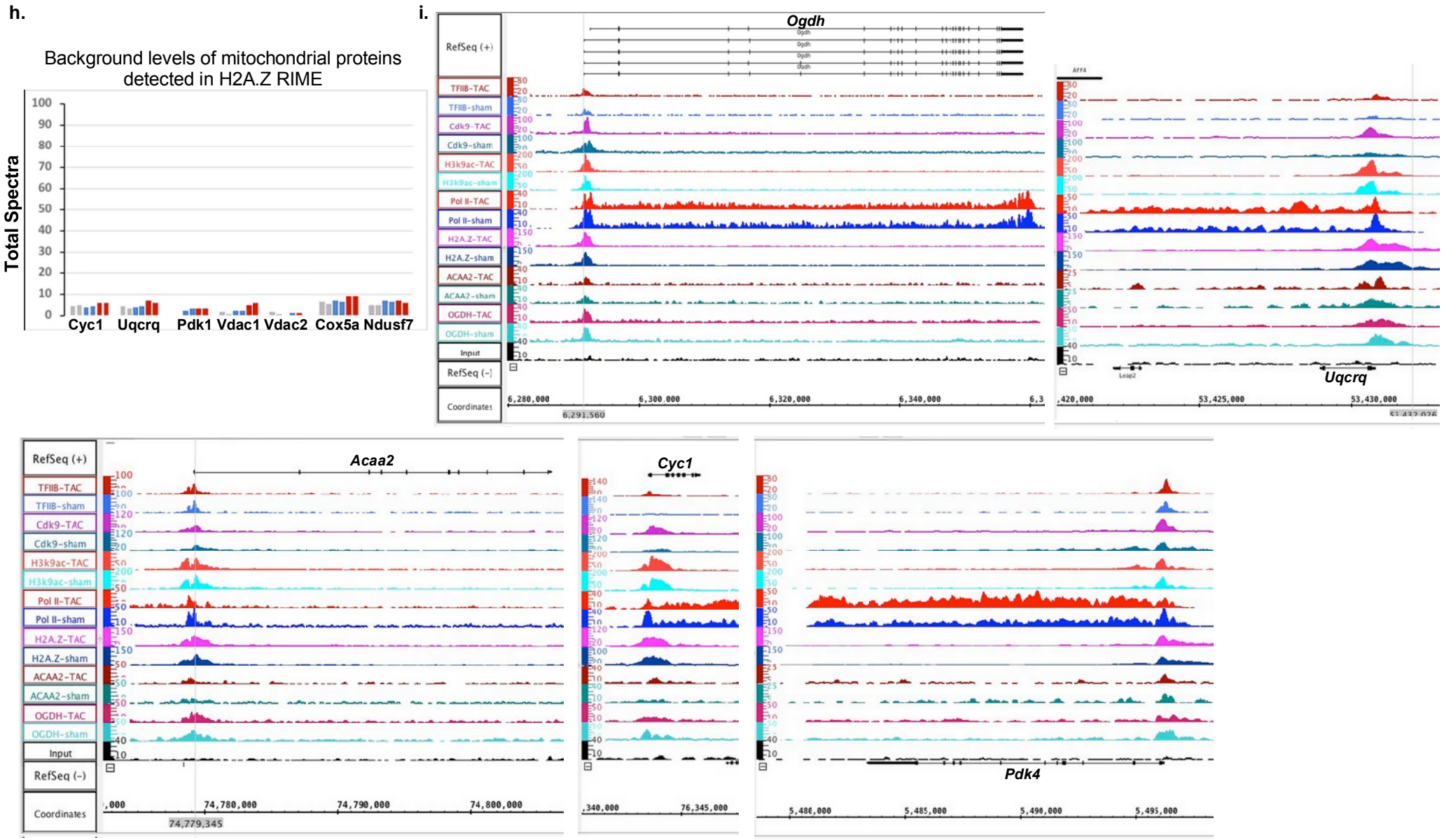

Figure 1S (h-i). Mitochondrial proteins, detected, but not enriched v. IgG in the H2A.Z RIME assay. **h.** Total spectra of a few of the mitochondria proteins identified in the IgG, sham, and TAC samples that included those with a cutoff of less than 2-fold enrichment v. control IgG, were plotted to demonstrate the selectivity of nuclear import of mitochondrial enzymes. These include respiratory complex proteins, mitochondrial membrane proteins, and pyruvate dehydrogenase kinases. **i.** Integrated genome browser images of the relative pol II occupancy across some of those genes relative to Acaa2 and Ogdh, reflecting comprable levels of transcriptional activity. Moreover, in spite of the relatively higher levels of PDK4 it was not detected in the RIME assay. These data suggest that the detection of mitochondrial proteins in the H2A.Z RIME assay was highly selective.

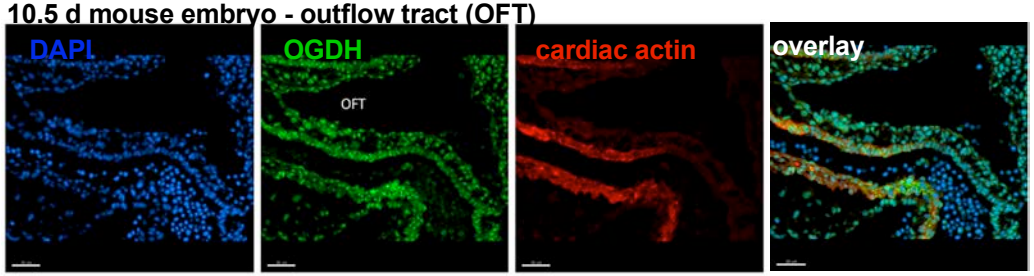

Figure 2S. Nuclear localization of OGDH in outflow tract of 10.5 d embryos. Ten and a half-day-old mouse embryos were immune-stained for OGDH (green), α-actinin (red), and DAPI (blue), each shown separately or in an overlay (rightmost). The scale bars represent 50 μm.

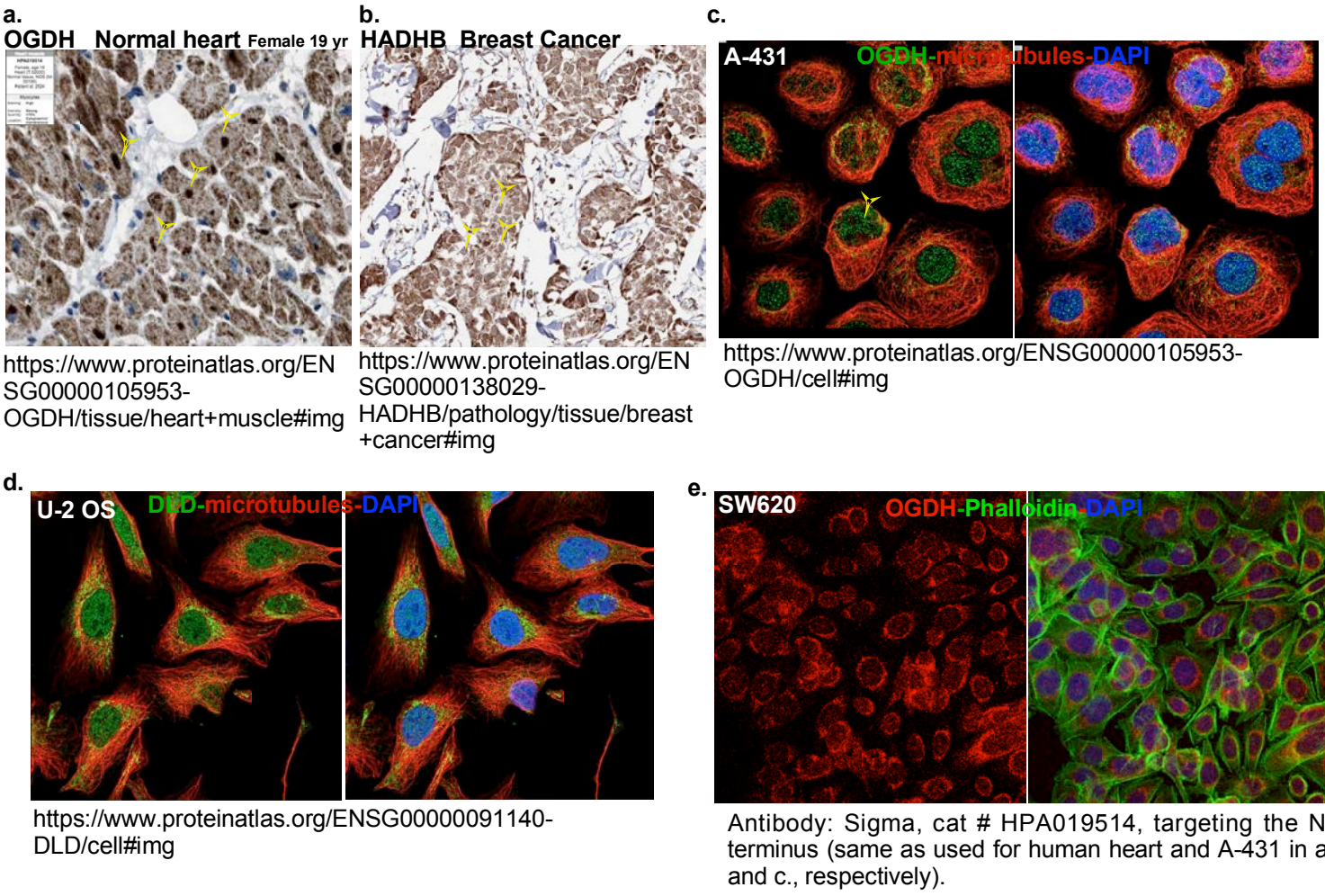

Figure 3S. Images from the human protein atlas project (www.proteinatlas.org) and repeat of OGDH immunostaining with a second antibody. The Human Protein Atlas is a Swedish-based project that includes antibody-based imaging of human tissue and cell lines, and is open access for scientists allowing free use of the data, given that it is properly cited [Ref. 30]. Shown are images from that project that include **a.** normal human heart sections immunostained with anti-OGDH, **b.** human breast cancer sections immunostained with anti-HADHB, **c.** A431 cells immunostained with anti-OGDH, and d. U-2 OS cells immunostained with anti-DLD. Direct links to the web pages are listed beneath each image. **e.** We also stained the human colon cancer cell line SW620 with the a second OGDH antibody that targets the N-terminus v. the C-terminus, used in main figure 2. Note, different antibodies had differential affinities to the nuclear v. mitochondrial form of a given protein, as demonstrated in our data

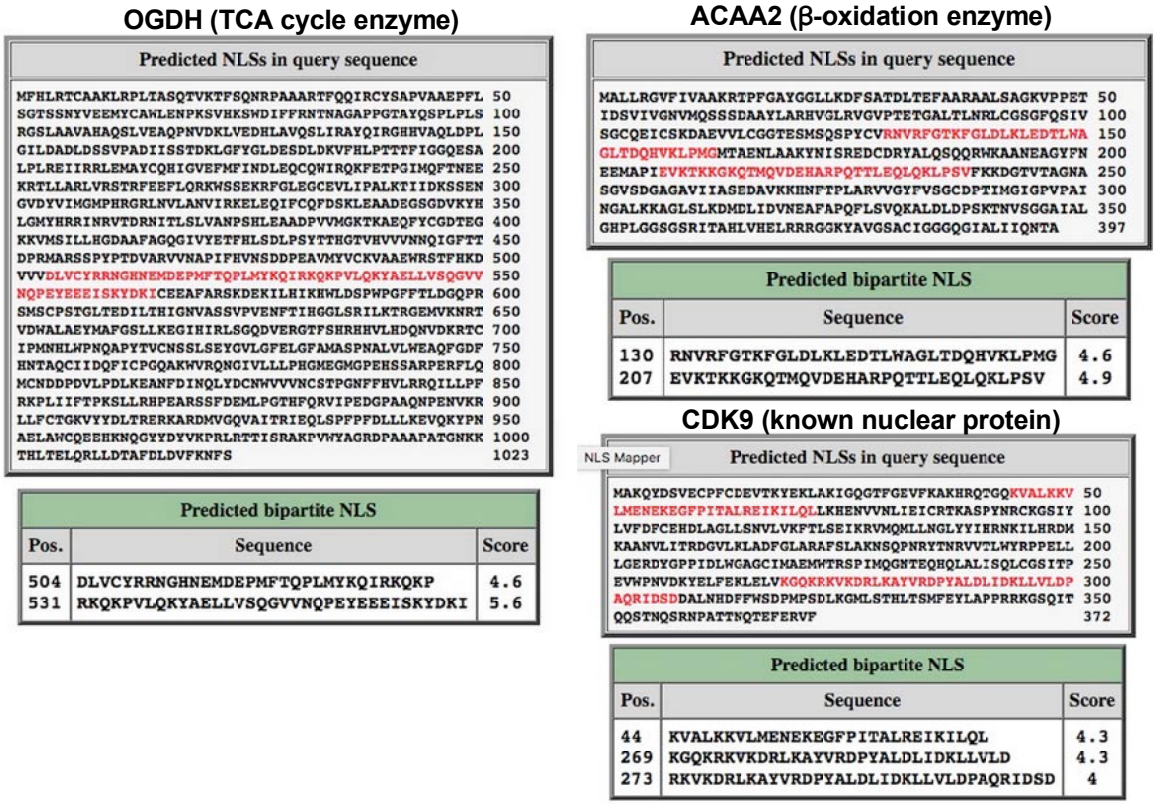

Mutations generated in the predicted NLS sequences:

OGDH a.a. 531-RKQKPVLQK mutated to RQQQPVLQQ

ACAA2 a.a. 207-EVKTKKGKQ mutated to EVQTQQGKQ

Figure 4S. Prediction of importin α-dependent nuclear localization signal (NLS) using cNLS Mapper. The images show the output of the NLS prediction results for OGDH, ACAA2, and CDK9 (used as a positive control), by cNLS Mapper, a free web-based prediction software: http://nls-mapper.iab.keio.ac.jp/cgi-bin/NLS_Mapper_form.cgi. The predicted NLS is indicated by red lettering. The scoring system is such that a protein with a score of 8, 9, or 10 is exclusively nuclear; 7 or 8 is partially nuclear; a score of 3, 4, or 5 is both nuclear and cytoplasmic; and a score of 1 or 2 is cytoplasmic. The mutations generated in the OGDH and ACAA2 predicted NLS are shown at the bottom, where the substituted R to Q residues are indicated in red.

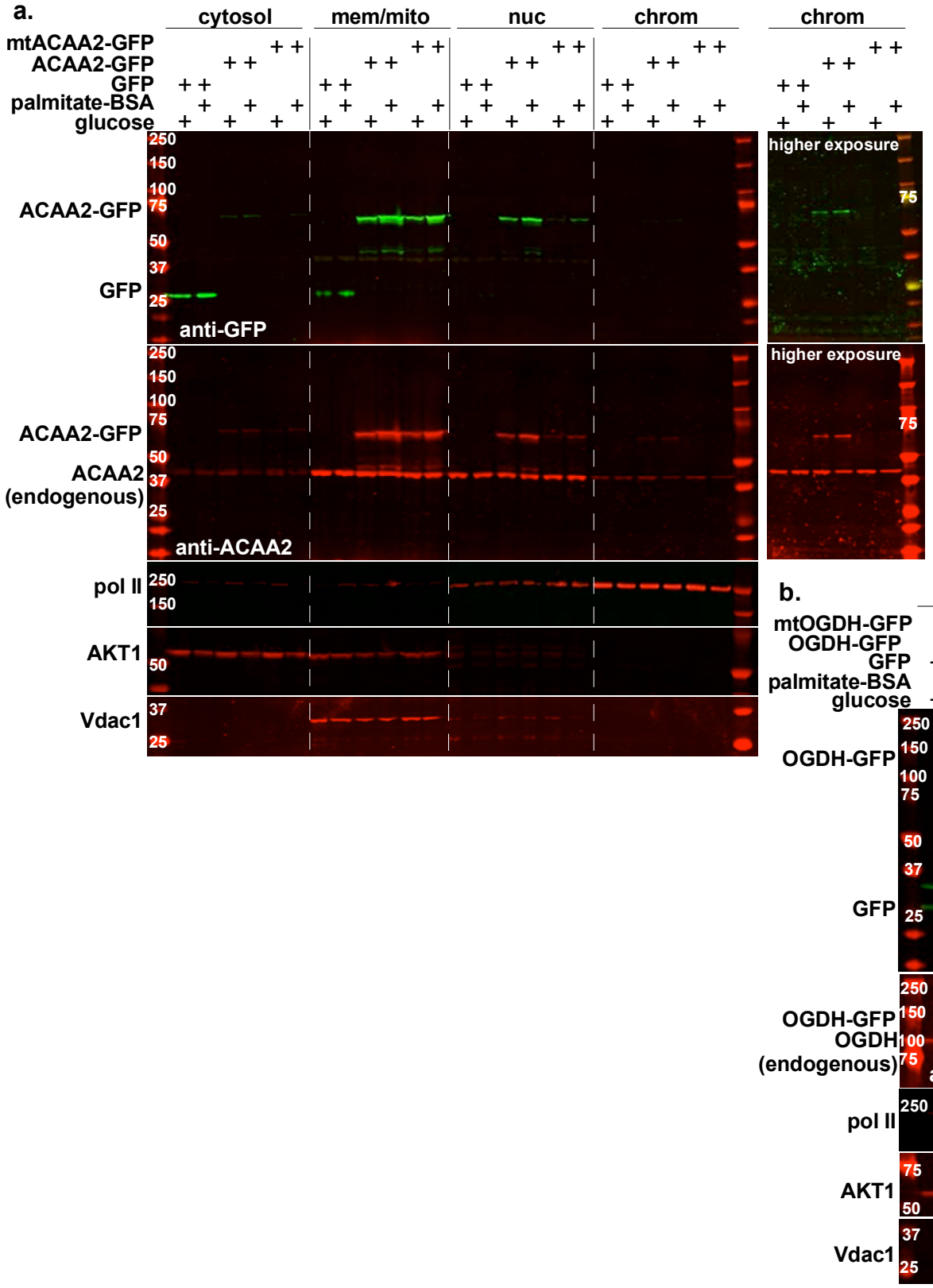

Figure 5S-a-b. Nuclear localization of ACAA2 and OGDH confirmed by tGFP-fusion proteins and NLS mutations. SW480 cells were infected with a 10-20 moi of recombinant adenoviruses harboring turbo-GFP (tGFP) or **a.** wt ACAA-tGFP or an NLS mutant (mtACAA2-tGFP), or **b.** wt OGDH or an NLS mutant (mtOGDH-tGFP). After 18 h, the cellular proteins were fractionated into cytosol (cyto), mitochondrial and membrane (mito), nucleoplasm (nuc), and chromatin-bound (chrom) protein fractions that were then analyzed by Western blotting for the proteins listed on the left of each panel. The fusion proteins were detected by anti-GFP (upper panels, a-b) and anti-ACAA2 or anti-OGDH (second from the top panels, a-b), which also detect the endogenous proteins. AKT1, VDAC1, and Pol II were immuno-detected for use as internal controls for the corresponding cell fractions.

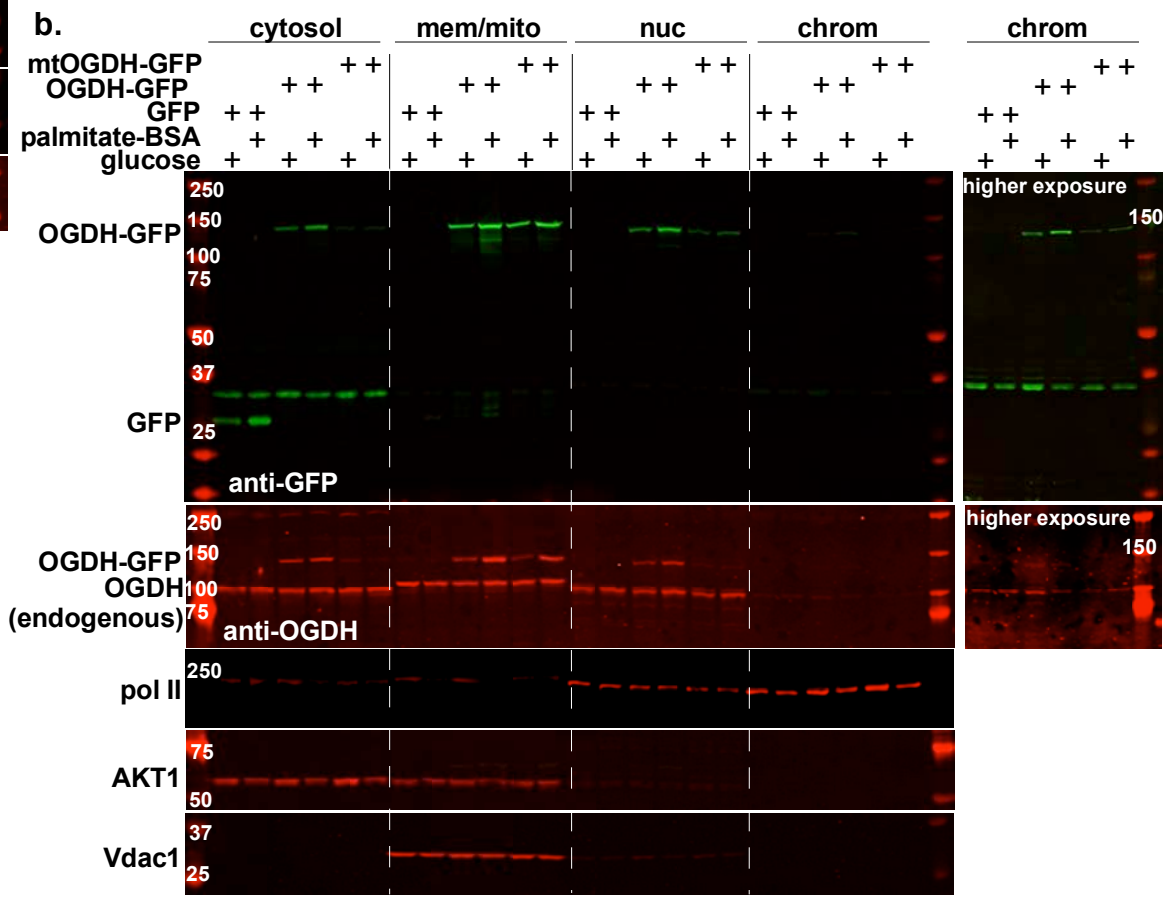

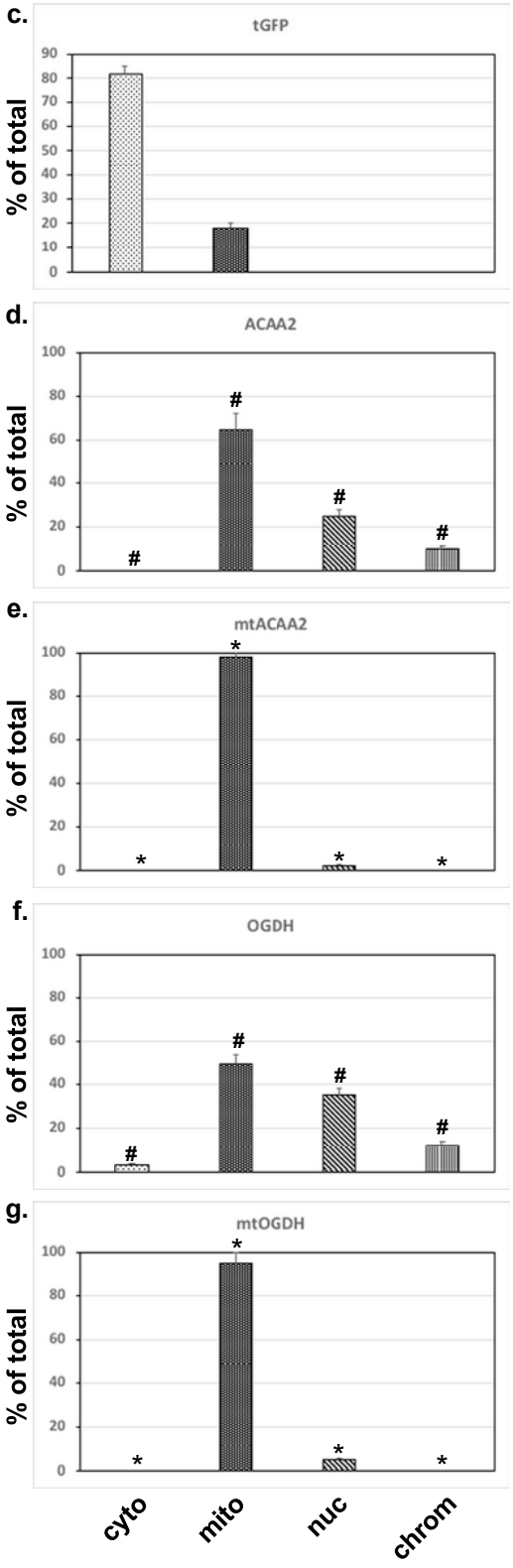

Figure 5S-c-g. The signals for the **c.** tGFP, and tGFP-fusion proteins **d.** ACAA2-tGFP, **e.** mtACAA2-tGFP, **f.** OGDH-tGFP, **g**. mtOGDH-tGFP, from the palmitate-BSA fed cells, were quantified using imageJ, normalized to internal controls, and plotted as the mean ± SEM of % total protein in all 4 fractions. Error bars represent SEM, N=3 from 3 repeats. #$p \leq 0.05$ vs. tGFP, *$p = 0.0095$ vs. wt tGFP-ACCA2 or -OGDH fusions, in corresponding fractions.

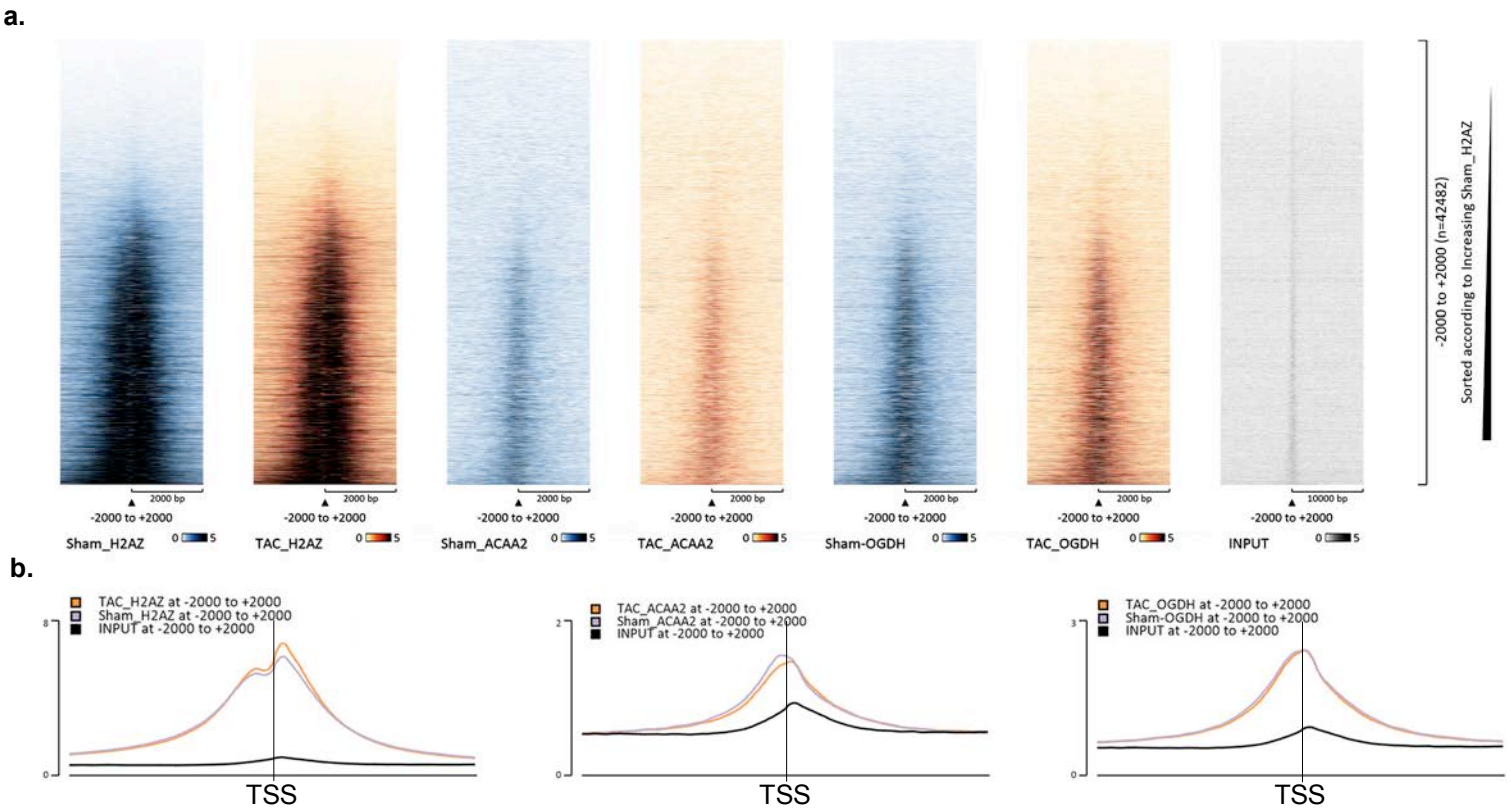

Figure 6S. The association of ACAA2 and OGDH with chromatin overlaps with H2A.Z at transcription start sites. Mice were subjected to a sham or TAC operation. One-week post-TAC, the hearts were isolated and analyzed by ChIP-Seq for H2A.Z, ACAA2, or OGDH (pool of 3, each). The sample size was determined based on the quantity of the material required for the assay and for biological averaging of samples based on our prior experience of the variability between mouse hearts in response to growth induction. a. Heatmaps of the ChIP-Seq sequence Tags from sham (blue), TAC (brown), and input (grey) aligned at the TSS. The y-axis represents individual positions of bins, and the x-axis represents a region from -2000 to +2000 bp relative to the TSS. b. Graphs representing average peak values of H2A.Z, ACAA2, and OGDH ChIP-Seq Tags from sham, TAC, and input from -2000 to +2000 bp relative to the TSS.

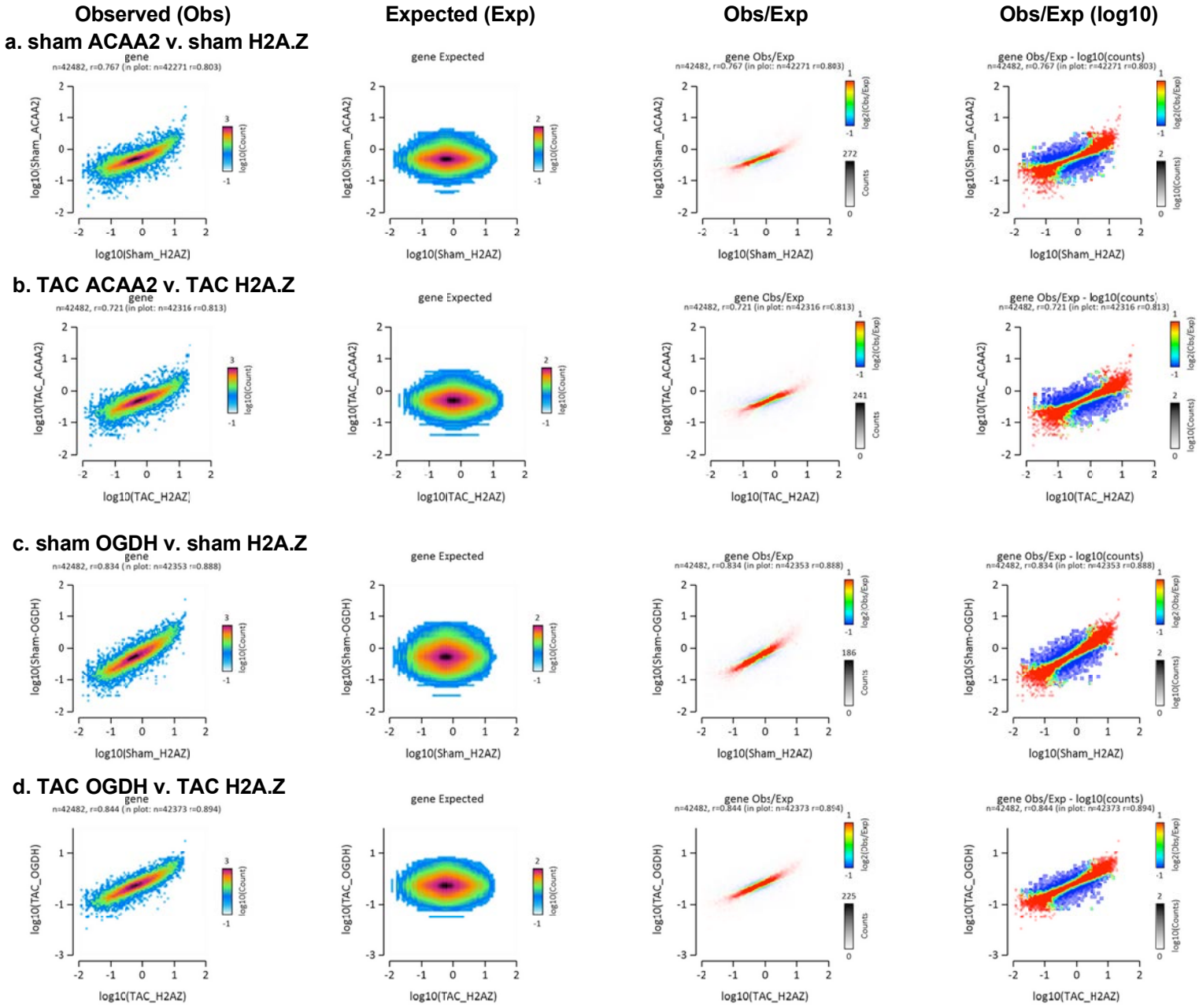

Figure 7S - The association of ACAA2 and OGDH with chromatin overlaps with H2A.Z at transcription start sites. Histograms showing the distribution of fragments calculated from their overall frequencies in the ChIP-Seq of H2A.Z (X-axis) v. ACAA2 or OGDH (Y-axis), and of ACAA2 (X-axis) v. OGDH (Y-axis), over the length of the gene and including -2000 bp upstream of the TSS, as labeled. The X and Y-axes were segmented into 75 bins, and the number of fragments within each bin was counted, color coded, and plotted. The bar to the right of the plot illustrates the relationship between count and coloring. The plots represent pseudo-colored 2D matrices showing observed, expected, and observed/expected distribution, calculated from the overall frequencies of fragments on each of the axes. These show the relation between **a.-b**. H2A.Z and ACAA2, **c.-d.** H2A.Z and OGDH, **e.-f.** ACAA2 and OGDH, **g.-h.** H2A.Z and H3K9ac, all in the sham and TAC hearts. The pseudo-color corresponds to the Obs/Exp ratio, and the color intensity is proportional to the log2 of the number of observed fragments within each bin. These plots suggest that there is a positive correlation between the levels of H2A.Z and ACAA2 or OGDH, where the red indicates that this occurs more frequently than expected by chance, as denoted by the correlation coefficient listed above each plot. **i.** A histogram showing the relation between H3K9ac and the input, as an example of unrelated binding events, and **j.** as an example of a perfect correlation. This figure was generated by EaSeq software.

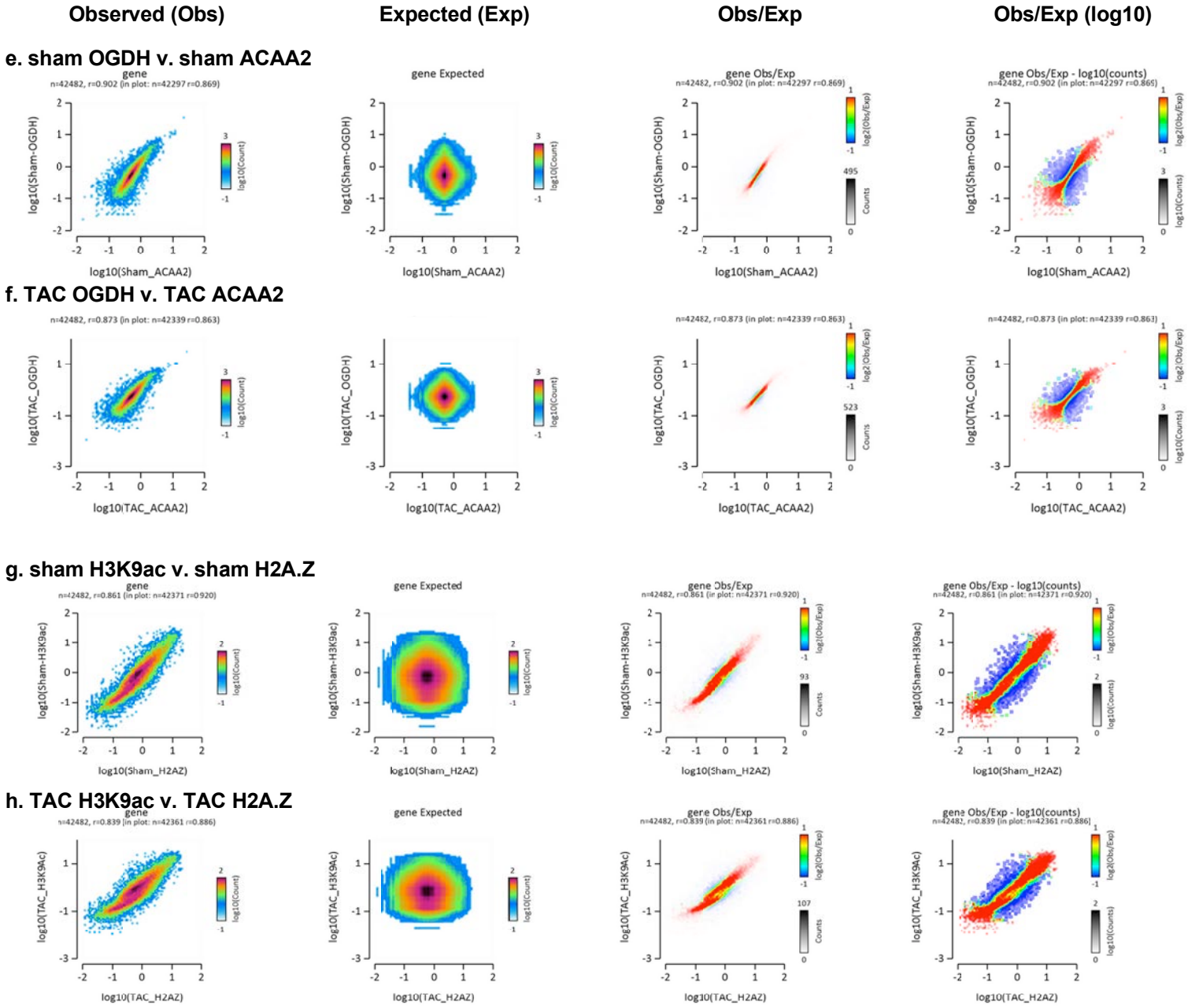

Figure 7S - continued

Observed (Obs) **Expected (Exp)** **Obs/Exp** **Obs/Exp (log10)**

i. unrelated event (TAC H3K9ac v. input)

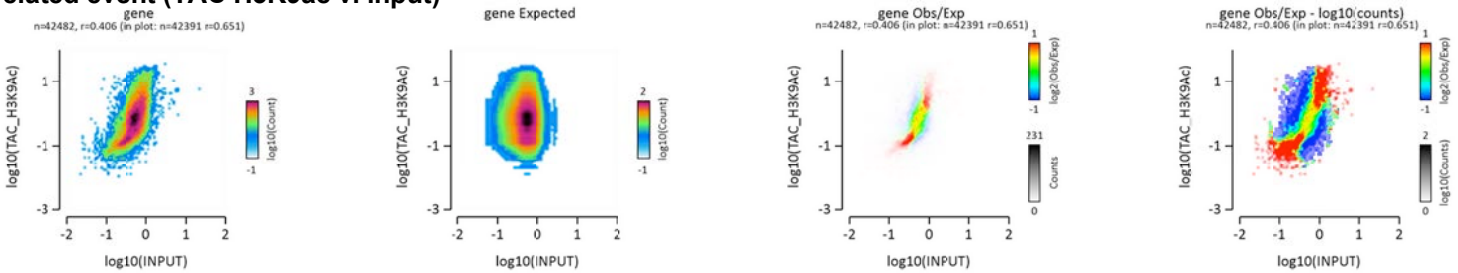

j. perfect overlap (TAC ACAA2 v. TAC ACAA2)

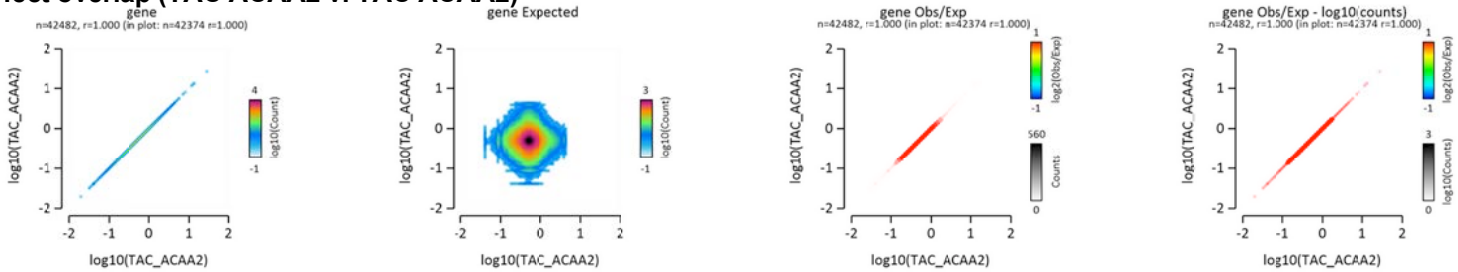

Figure 7S - continued

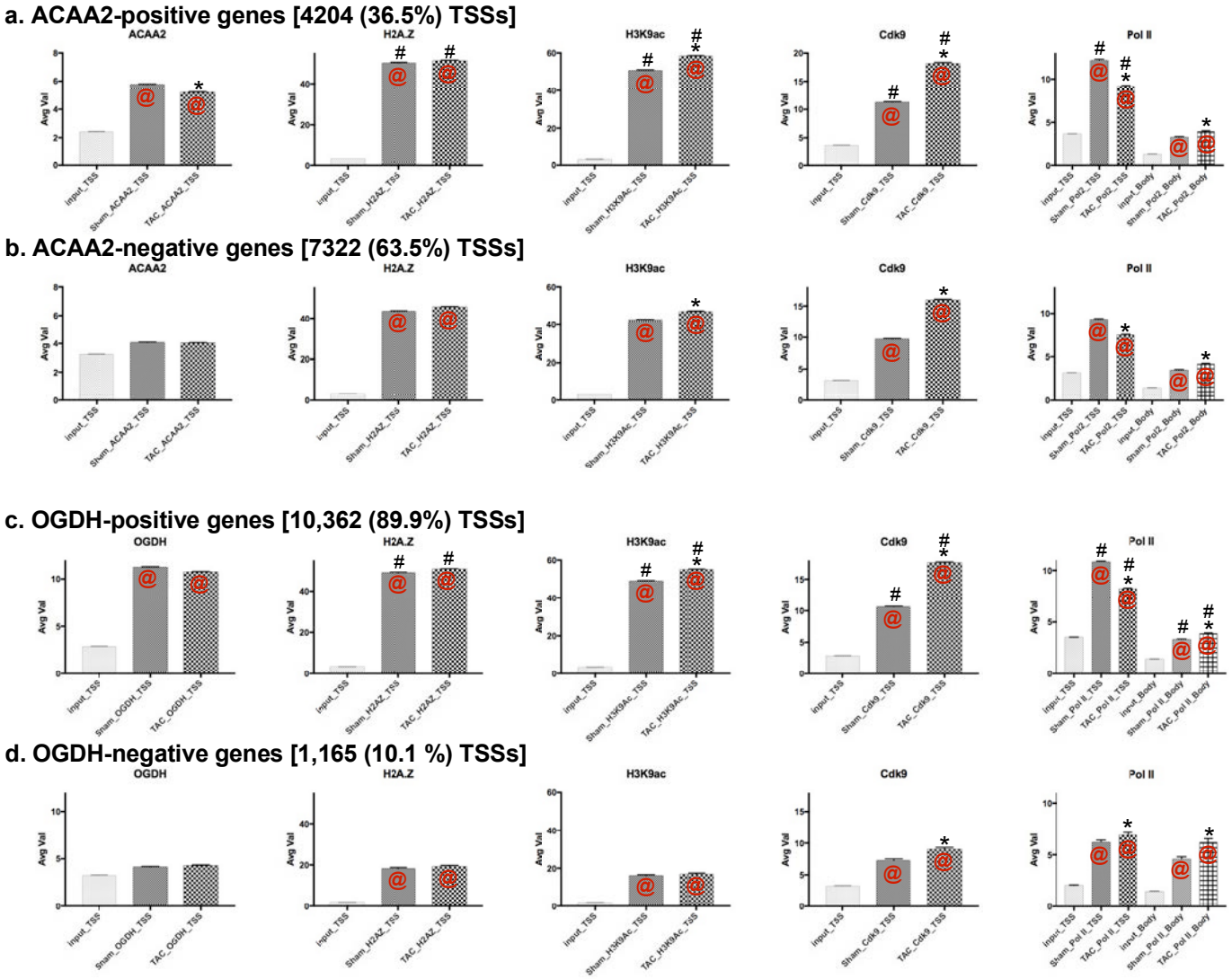

Figure 8S-a-d. The mean for the average values of sequence Tags at the TSS of ACAA2- and OGDH-, positive and negative genes. Mice were subjected to a sham or TAC operation to induce hypertrophic growth. One-week post-TAC, the hearts were isolated and analyzed by ChIP-Seq for ACAA2 or OGDH. Expressed genes (RNA pol II positive) were sorted into 4 groups: a. ACAA2-positive, b. ACAA2-negative, c. OGDH-positive, and d. OGDH-negative. The mean of the average values (AvgVal) of sequence Tags for ACAA2, OGDH, H2A.Z, H3K9ac, Cdk9, and pol II, at the TSS and gene body (pol II only), were calculated and plotted. Error bars represent standard error of the mean, and * = $p \leq 0.05$ v. sham in the same plot, # = $p \leq 0.05$ v. corresponding data point in the ACCA2-negative or OGDH negative plot, @ = $p \leq 0.05$ v. input.

e. ACAA2, upregulated during cardiac growth (>1.25-fold, 697 TSSs)

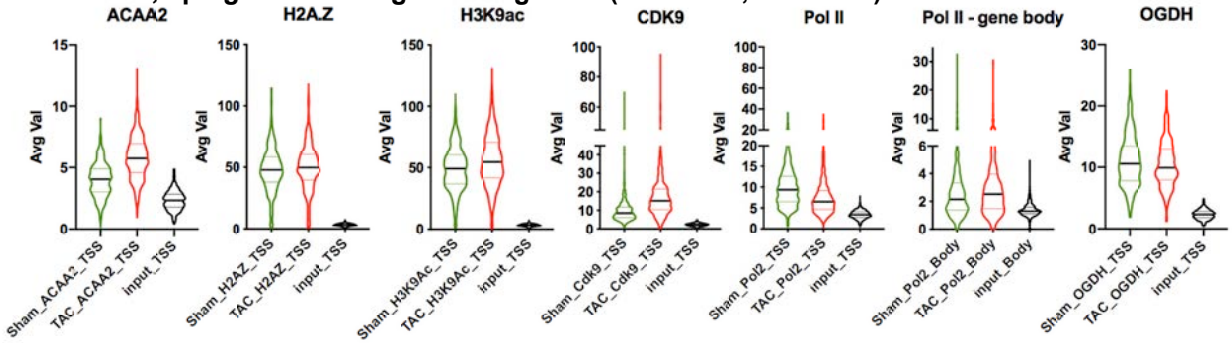

f. ACAA2, downregulated during cardiac growth (<0.75-fold, 1203 TSSs)

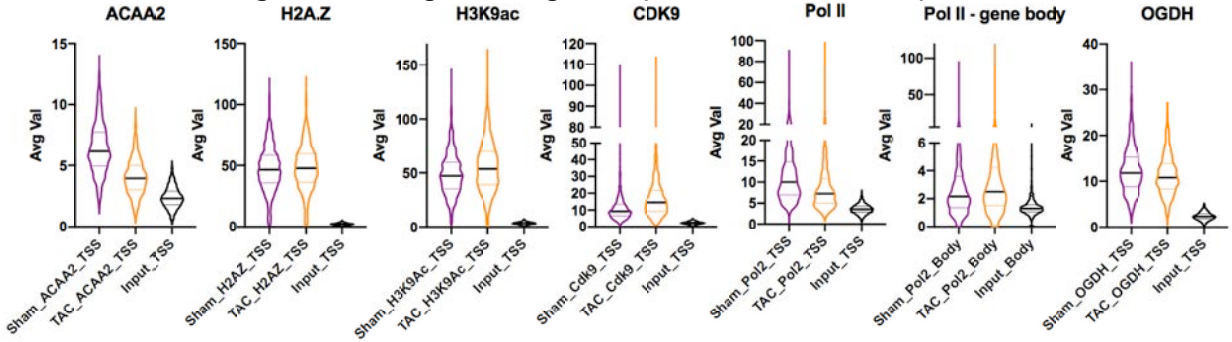

g. OGDH, upregulated during cardiac growth (>1.25-fold, 992 TSSs)

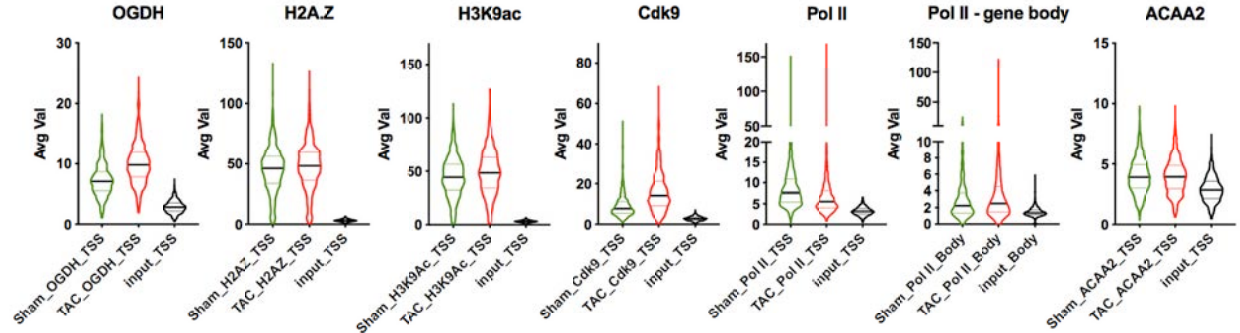

h. OGDH, downregulated during cardiac growth (<0.75-fold, 993 TSSs]

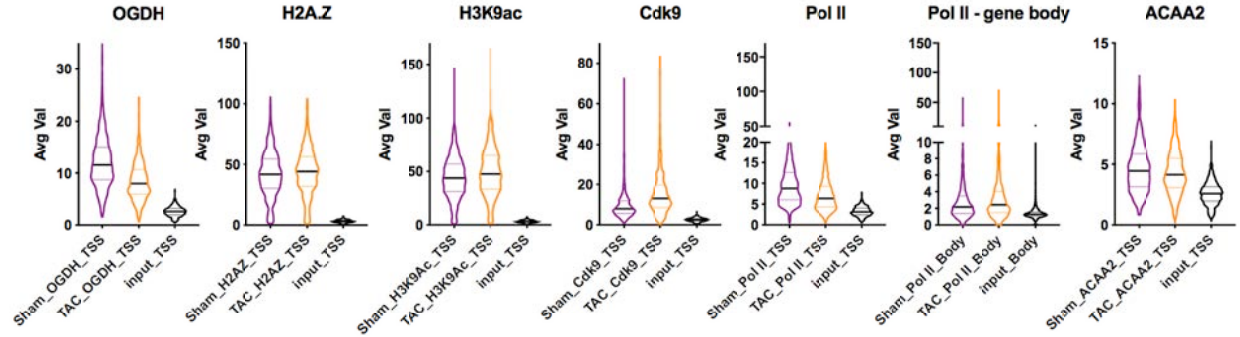

Figure 8S-e-h. Mice were subjected to a sham or TAC operation to induce hypertrophic growth. One-week post-TAC, the hearts were isolated and analyzed by ChIP-Seq for ACAA2 or OGDH. Using the sequence tags, expressed genes (pol II-positive) were sorted into: a. ACAA2-positive that exhibit upregulation during growth, b. ACAA2-positive that exhibit downregulation during growth, c. OGDH-positive that exhibit upregulation during growth, and d. OGDH-positive that exhibit downregulation during growth. The sequence tags were sorted in parallel with the sequence tags from H2A.Z, H3K9ac, Cdk9, pol II, and OGDH ChIP-Seq, at the TSS (-1000 to + 1000). The results were plotted as violin plots, in which the horizontal solid line represent the median, and the dashed lines the quartiles, and the shape of the violin reflects the tags' density distribution.

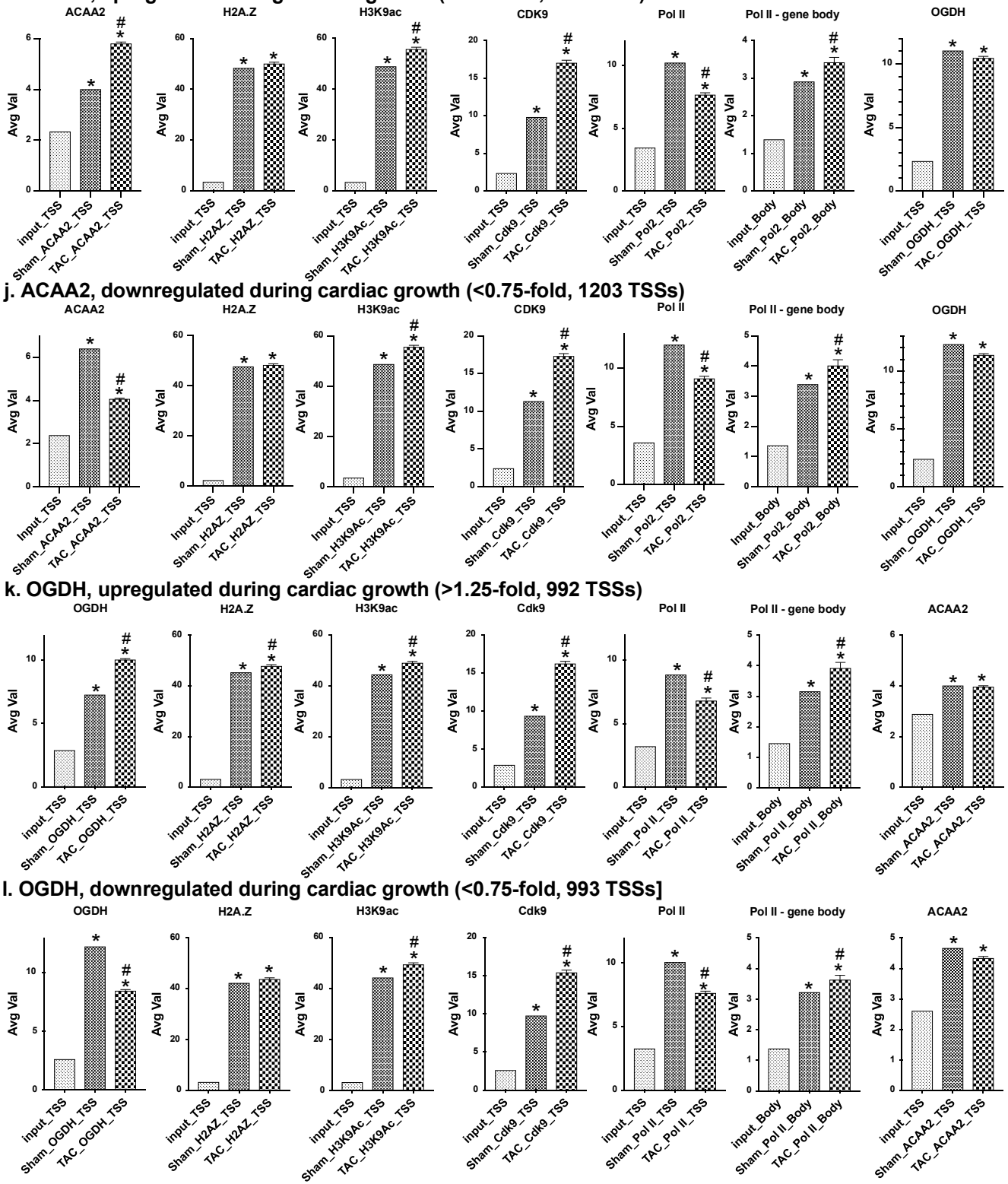

Figure 8S-i-l. The mean for the average values of sequence Tags at the TSS of genes exhibiting upregulation or downregulation of ACAA2 or OGDH during cardiac growth. Mice were subjected to a sham or TAC operation to induce hypertrophic growth. One-week post-TAC, the hearts were isolated and analyzed by ChIP-Seq for ACAA2 or OGDH. Expressed genes (RNA pol II positive) were sorted into 4 groups: a. ACAA2 upregulated, b. ACAA2 downregulated, c. OGDH upregulated, and d. OGDH-negative, during cardiac growth. The mean of the average values (Avg Val) of sequence Tags for ACAA2, OGDH, H2A.Z, H3K9ac, Cdk9, and pol II, at the TSS and gene body (pol II only), were calculated and plotted. Error bars represent standard error of the mean, and * = $p \leq 0.05$ v. input in same plot, # = $p \leq 0.05$ v. sham in the same plot.

a.

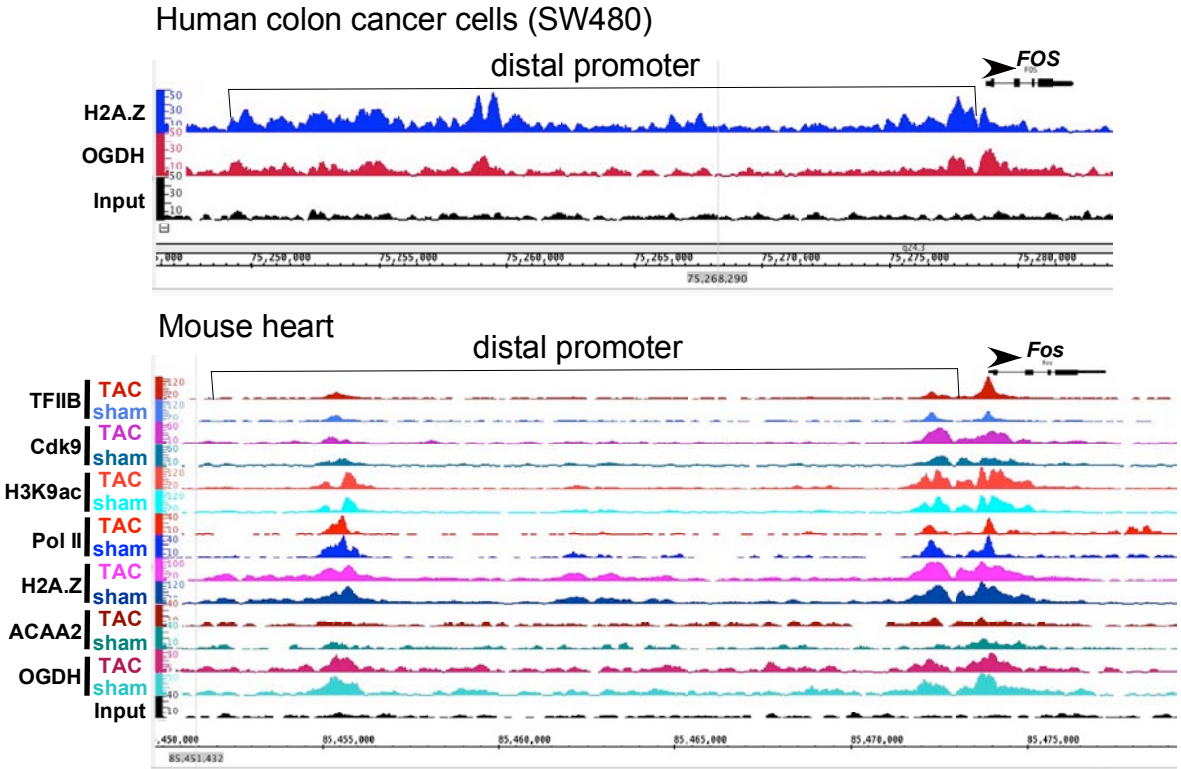

Figure 9S-a. OGDH and ACAA2 differentially overlap with H2A.Z at distal promoter regions of inducible genes. The human SW480 colon cancer cell line, was subjected to H2A.Z and OGDH ChIP-Seq using the same antibodies and chromatin concentration applied in the mouse heart tissue ChIP-Seq. The resulting sequence tags from both reactions (y-axis) were aligned across the genome's coordinates (x-axis). The results show the distal promoter region of the human and mouse *FOS* genes.

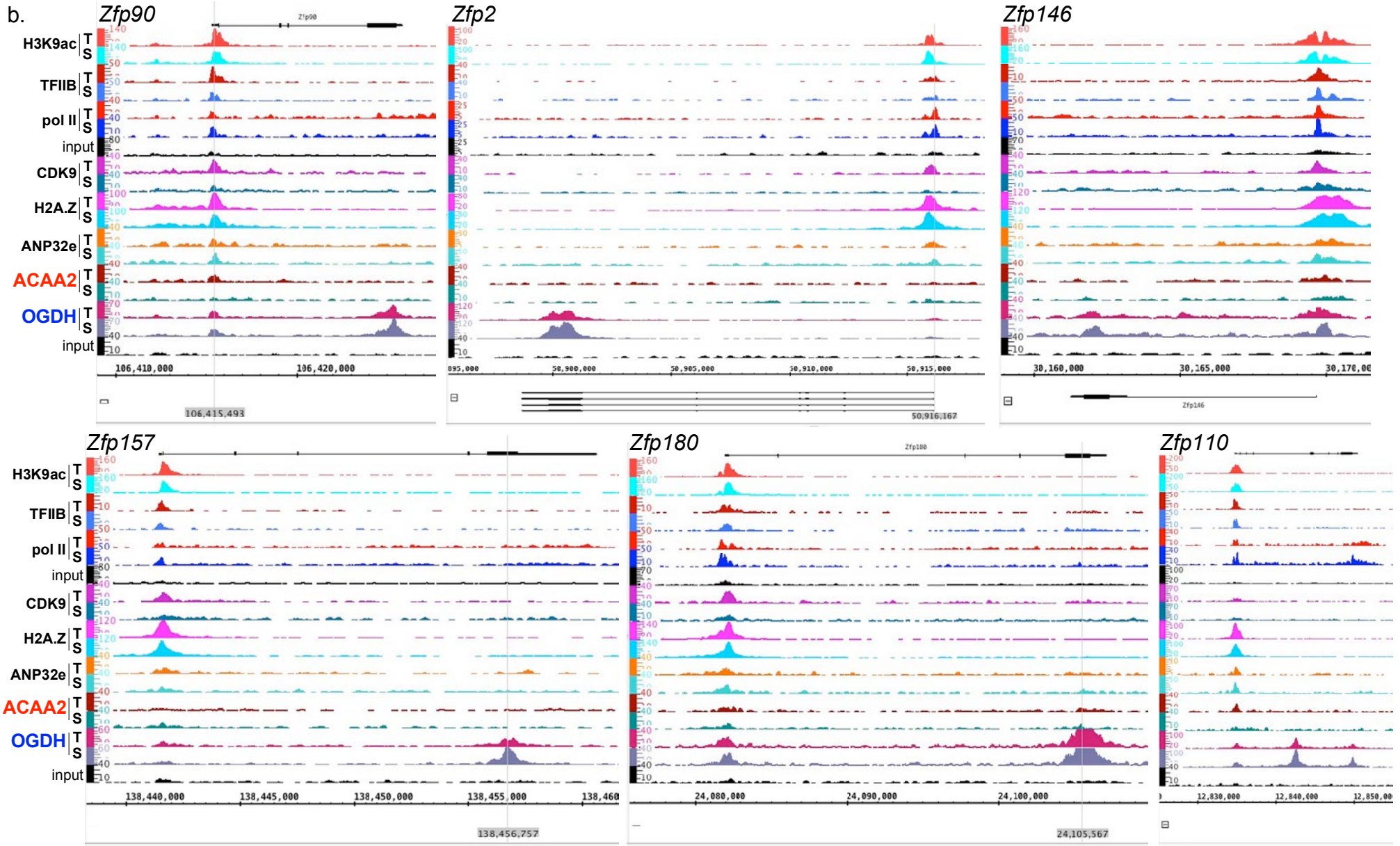

Figure 9S-b. OGDH binds to the terminal exons of zinc finger proteins, in a H2A.Z-independent manner. The alignment of the ChIP-Seq sequence tags for H3K9ac, TFIIB, pol II, Cdk9, H2A.Z, ANP32E, ACAA2, and OGDH (y-axis) across the genomic coordinates (x-axis) of *Zfp90, Zfp2, Zfp146, Zfp157, Zfp180, and Zfp110 genes*. The arrow shows the start and direction of transcription. The results show a substantial peak of OGDH in the terminal exons of these genes that is subject to differential regulation during cardiac hypertrophy. In addition, all genes show OGDH at their TSSs, albeit at a lower density.

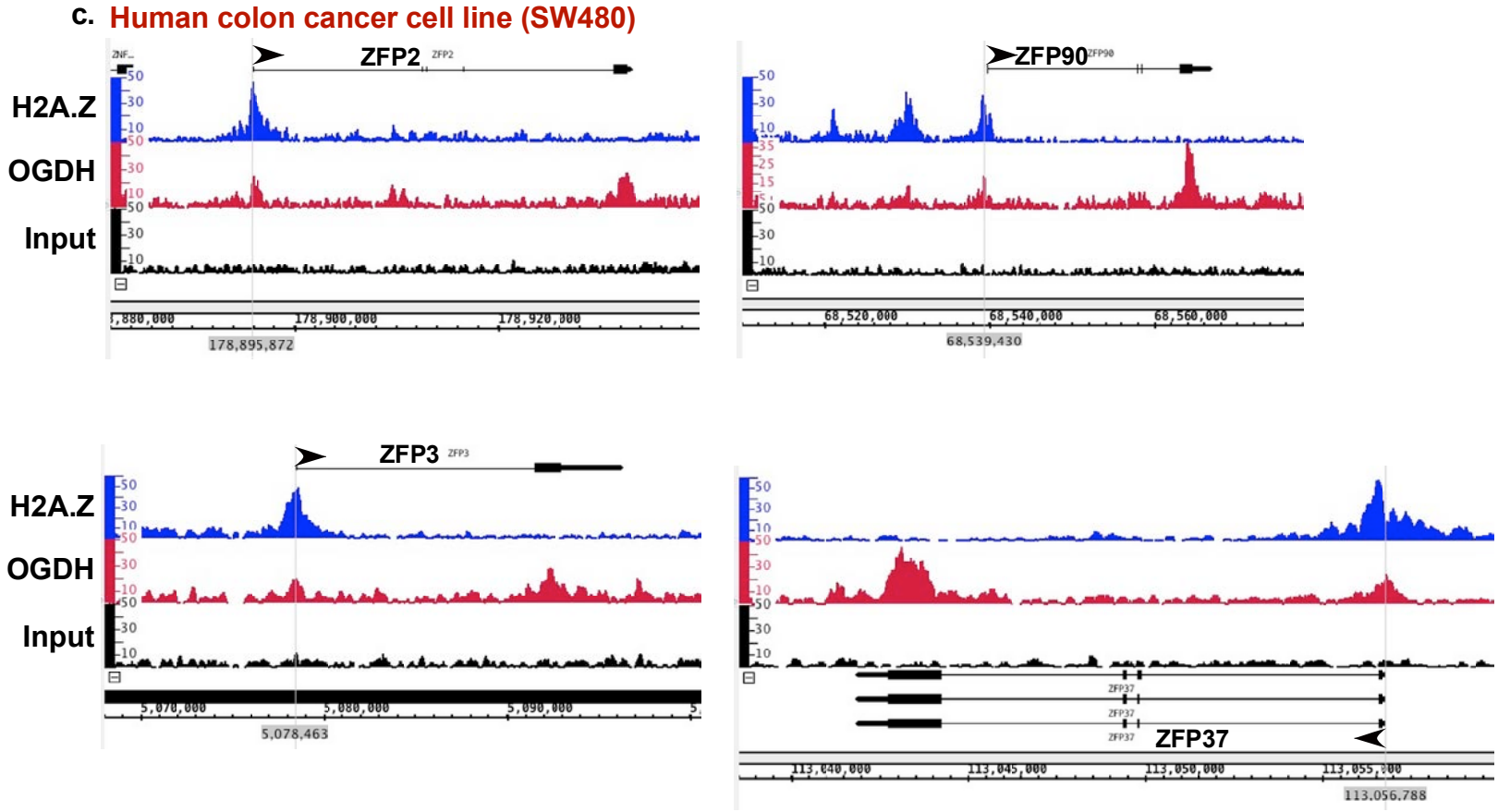

Figure 9S-c. H2A.Z-independent binding of OGDH to the terminal exon in ZFP genes in humans. The human SW480 colon cancer cell line, was subjected to H2A.Z and OGDH ChIP-Seq using the same antibodies and chromatin concentration applied in the mouse heart tissue ChIP-Seq. The resulting sequence tags from both reactions (y-axis) were aligned across the genome's coordinates (x-axis). The results show 4 examples of ZFP genes in which OGDH is present in their terminal exon in the absence of H2A.Z, similar to what we observed in the mouse tissue (see Fig. 8S).

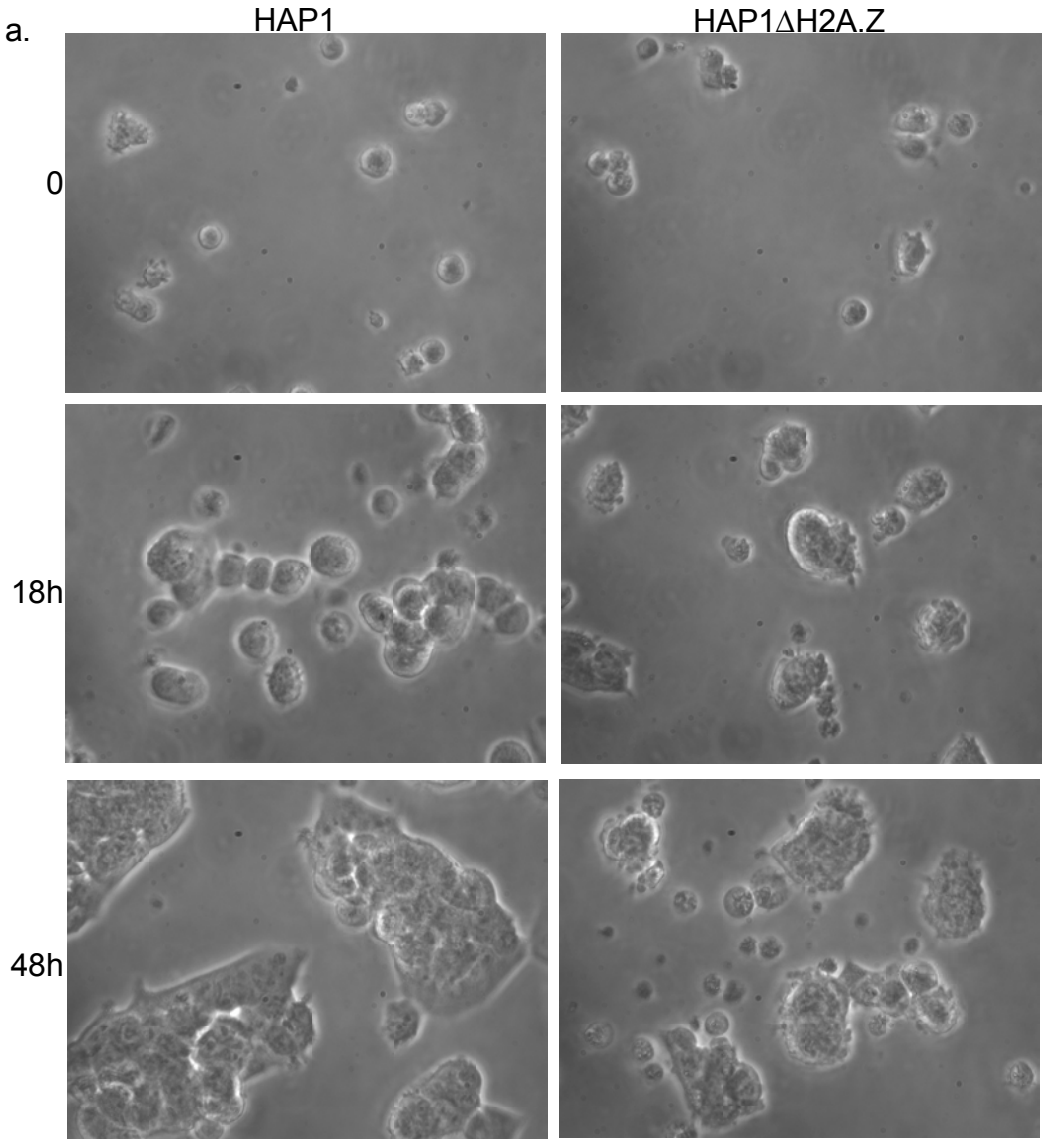

Fig. 10S. HAP1ΔH2A.Z are viable but proliferate at a slower rate than the parent cells. HAP1 and HAP1ΔH2A.Z were purchased from Horizon Discovery and cultured according to the company's protocol on gelatin coated glass slides. On day 0 equal number of cells were seed and imaged live at 18 and 48 h after that. Cells were counted at each time point in 3 fields revealing a ~4:1 ratio of parent:ΔH2A.Z cell numbers.

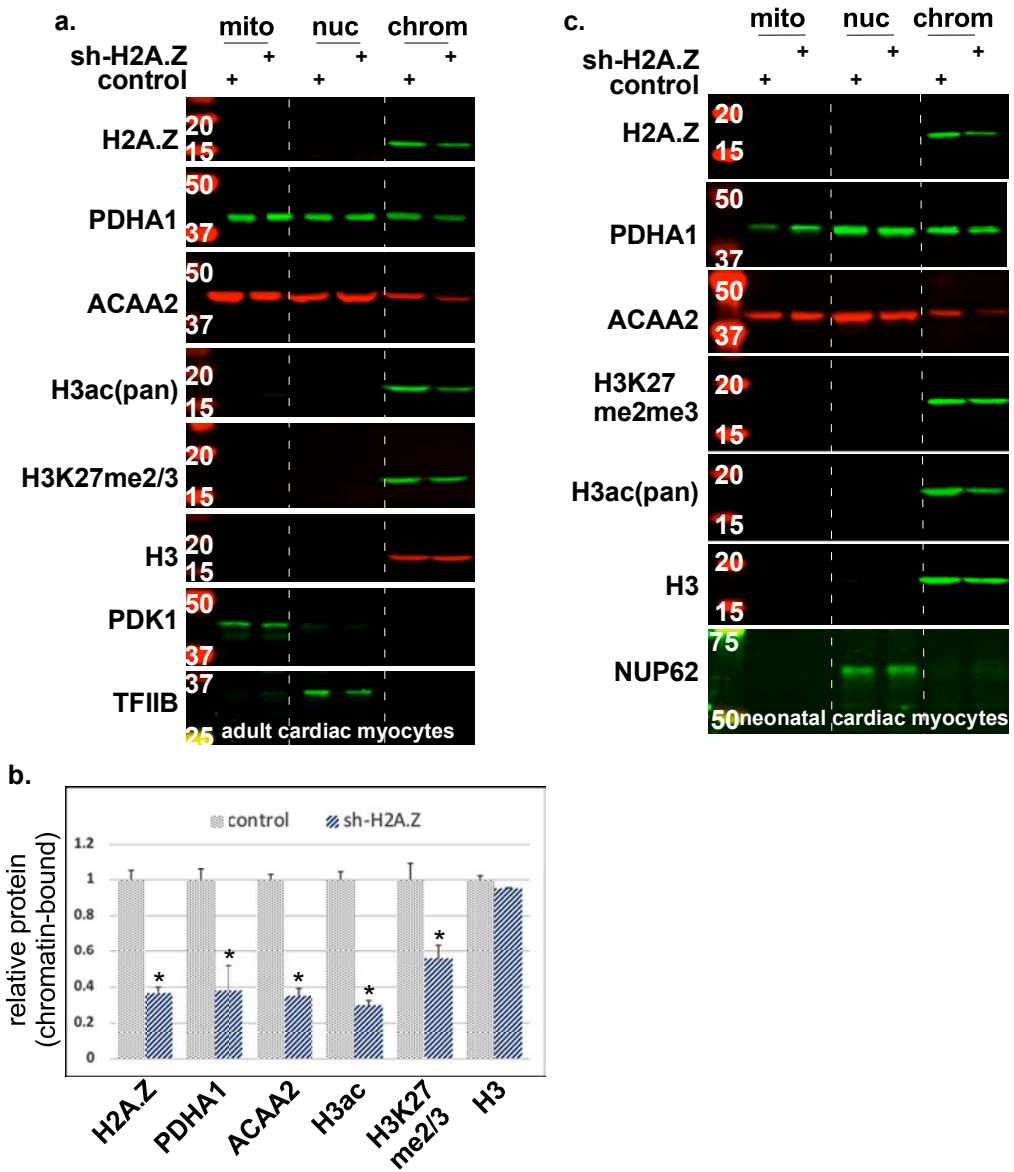

Figure 11S. Knockdown of H2A.Z inhibits chromatin binding of metabolic enzymes and reduces histone modifications. Rat neonatal cardiac myocytes were isolated from the hearts of 1 day old Sprague Dawley pups. They were then infected with 30 moi of adenoviruses harboring a nonsense shRNA control or one targeting H2A.Z. After 24 h, organelles were isolated and fractionated into membrane/mitochondrial (mem), nuclear (nuc), and chromatin-bound (chrom, no crosslinking applied), using a combination of differential lysis and sequential centrifugation. The proteins extracted from each of these fractions were analyzed by Western blotting for the genes indicated on the right of each panel.

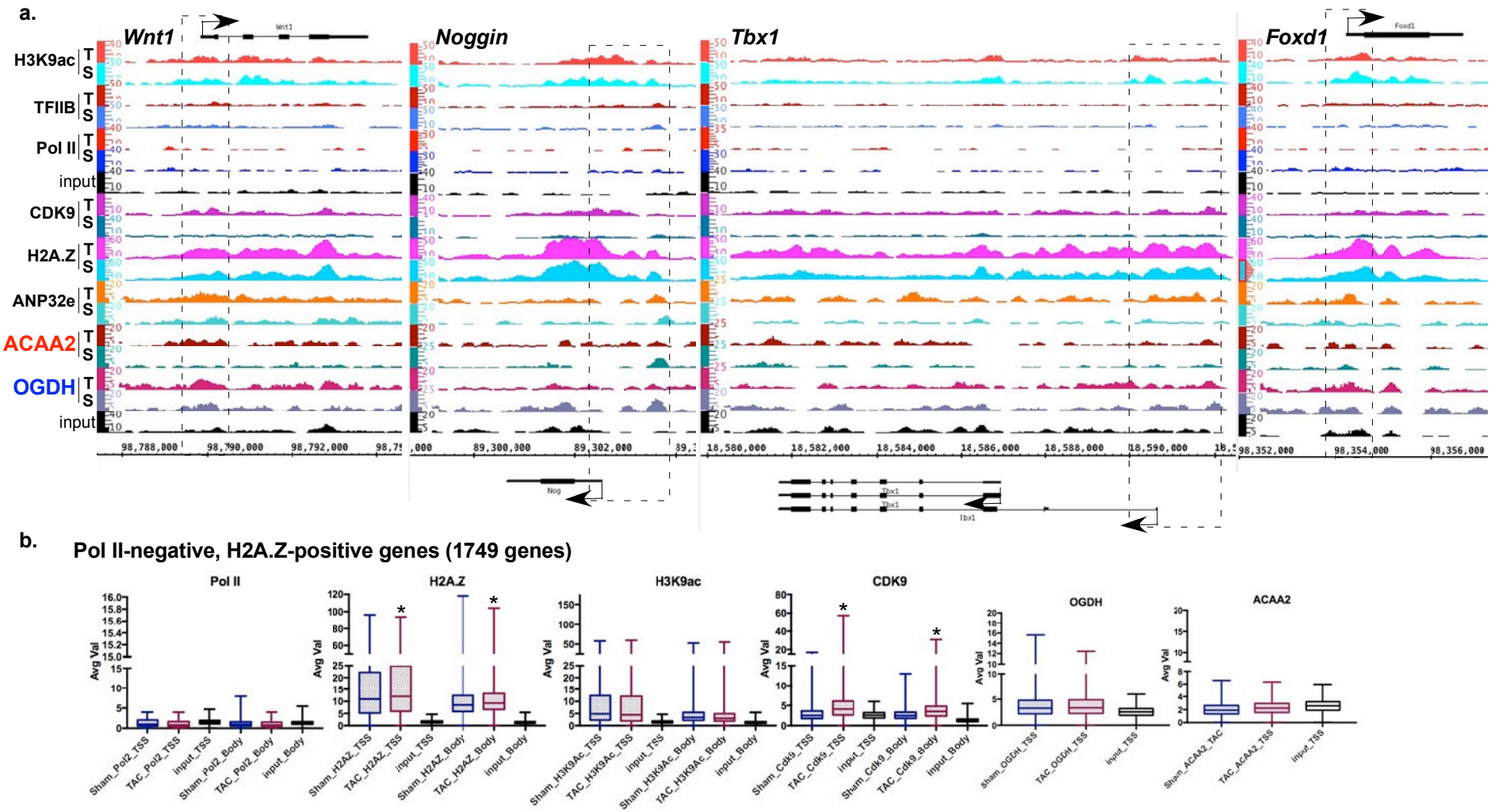

Figure 12S. H2A.Z associates with the suppressed development genes. Mice were subjected to a sham or TAC operation. One-week post-TAC, the hearts were isolated and analyzed by ChIP-Seq for ACAA2. **a.** The alignment of the ChIP-Seq sequence Tags for H3K9ac, TFIIB, pol II, Cdk9, H2A.Z, ANP32E, ACAA2, and OGDH across the genomic coordinates of *Wnt1*, *Noggin*, *Tbx1*, and *Foxd1*, developmental genes. **b.** Genes were sorted for those that were pol II-negative genes and H2A.Z-posirive. The ChIP-Seq sequence Tags for ACAA2, H2A.Z, H3K9ac, OGDH, and pol II, at the TSS (-1000 to +1000) and across the gene body (+1000-gene end), were plotted as box plots (median and quartiles).